LAWRENCE
LIVERMORE
NATIONAL
LABORATORY

LLNL-JRNL-590392

A Detailed Kinetic Modeling Study of n-Pentanol Oxidation

K. A. Heufer, S. M. Sarathy, H. J. Curran, A. C. Davis, C. K. Westbrook, W. J. Pitz

October 11, 2012

Energy & Fuels

Disclaimer

A Detailed kinetic modeling study of n-pentanol oxidation

Journal:	*Energy & Fuels*
Manuscript ID:	ef-2012-012596.R1
Manuscript Type:	Article
Date Submitted by the Author:	n/a

Complete List of Authors:	Heufer, Karl; National University of Ireland Galway, Combustion Chemistry Centre Sarathy, Mani; King Abdullah University of Science and Technology, Clean Combustion Research Center Curran, Henry; NUI, Galway, Chemistry Davis, Alexander; King Abdullah University of Science and Technology, Clean Combustion Research Center Westbrook, Charles; Lawrence Livermore Laboratories, Pitz, William; Lawrence Livermore National Laboratory, Chemistry, Material, and Life Sciences Directorate

A Detailed kinetic modeling study of *n*-pentanol oxidation

K. Alexander Heufer[†*], S. Mani Sarathy[‡], Henry J. Curran[†], Alexander C. Davis[‡], Charles K. Westbrook[▯], William J. Pitz[▯]

[†]*National University of Ireland Galway, University Road, Galway, Ireland*

[‡]*Clean Combustion Research Center, King Abdullah University of Science and Technology, Thuwal, Kingdom of Saudi Arabia*

[▯]*Lawrence Livermore National Laboratory, 7000 East Avenue, Livermore, California, USA*

KEYWORDS. Kinetic modeling, pentanol, alcohol, biofuel

ABSTRACT. To help overcome the world's dependence on fossil fuels, suitable biofuels are promising alternatives that can be used in the transportation sector. Recent research in internal combustion engines shows that short alcoholic fuels (e.g. ethanol or *n*-butanol) have reduced pollutant emissions and increased knock resistance compared to fossil fuels. Although higher molecular weight alcohols (e.g. *n*-pentanol and *n*-hexanol) exhibit higher reactivity that lowers their knock resistance, they are suitable for diesel engines or advanced engine concepts, like HCCI, where higher reactivity at lower temperatures is necessary for engine operation. The present study presents a detailed kinetic model for *n*-pentanol based on modeling rules previously presented for *n*-butanol. This approach was initially validated using quantum chemistry calculations to verify the most stable *n*-pentanol conformation and to obtain C–H and C–C bond dissociation energies. The proposed model has been validated against ignition delay time data, speciation data from a jet stirred reactor, and laminar

flame velocity measurements. Overall, the model shows a good agreement to the experiments and permits a detailed discussion of the differences between alcohols and alkanes.

INTRODUCTION. One of the major challenges of the 21st century is to overcome man's dependence on fossil fuels. This is motivated, not only by the fact that the foreseen scarcity of fossil fuels will lead to a significant increase in energy costs, but also by the inevitable increase in anthropogenic greenhouse gas emissions associated with fossil fuel combustion leading to current research for less carbon intensive sources for energy.

A possible alternative for fossil fuels in the transport sector are suitable biofuels produced from renewable sources. Today's first generation biofuel, ethanol, is widely used as a pure fuel or as a fuel additive. Although ethanol has the potential to reduce both the dependency on petroleum based fuels, and the amount of anthropogenic greenhouse gas emissions (1), this fuel suffers from disadvantages such as a low energy density, a high hygroscopicity, and a high volatility. Nevertheless, the use of ethanol as an alternative fuel is a first step towards the aim of finding a secure and clean solution for the world's energy demand.

Many studies have investigated the combustion characteristics of ethanol in experiments and kinetic simulations (2–8). Ethanol shows a higher reactivity at high temperatures compared to typical *n*-alkanes, e.g. *n*-heptane, but a lower reactivity at lower temperatures. For this reason, ethanol suppresses uncontrolled autoignition (i.e. knock) in spark ignition (S.I.) engines and is used as an octane improver. Nevertheless, ethanol shows a tendency to pre-ignite in shock tube experiments, which can significantly reduce ignition delay times at lower temperatures (8). The process leading to pre-ignition is, as yet, not fully understood but might be linked to pre-ignition phenomena, also observed in engine experiments that can lead to critical damage during engine operation.

Alternatively, butanol can be used in gasoline engines and again several studies can be found investigating its combustion characteristics (9–13). Butanol has the advantage of having a higher

energy density, lower hygroscopicity, and lower volatility, compared to ethanol. The reactivity at high temperatures is similar to ethanol and at low temperatures only a slight increase in the reactivity is observed. Thus, as ethanol, it can be used as an octane improver. Furthermore, pre-ignition seems to be significantly less likely for butanol, based on shock tube experiments, (14) which could be an additional advantage for the use of butanol in spark ignition engines. A comprehensive overview of butanol oxidation literature can be found in (15) where a detailed kinetic model for all four butanol isomers is also presented, explaining in detail the features of C_4 alcohol chemistry.

Although shorter alcoholic fuels with low reactivity increase knock resistance in S. I. engines, longer alcoholic fuels with a higher reactivity are interesting alternative fuels for other types of engines. Low temperature activity is needed for autoignition in diesel engines and in modern engine concepts like Homogeneous Charge Compression Ignition (HCCI). These higher molecular weight alcohols can also be produced from renewable sources (16–19). A recent study of *n*-pentanol and *n*-hexanol shows an alkane-like negative temperature coefficient (NTC) behavior for these fuels (20). That study suggested that a longer carbon chain in an alcoholic fuel causes its reactivity to be closer to that of its corresponding alkane. Furthermore, studies of these fuels in a jet-stirred reactor (JSR) and in a combustion bomb can be found in the literature (21, 22). Engine experiments performed with these fuels show a superior performance regarding pollutant emissions, compared to pure petroleum based fuels (23–26). For example, a Cooperative Fuel Research (CFR) engine study (26) showed that gasoline fuel blended with mixtures of C1–C5 alcohols had improved knock resistance, but increasing the amount of *n*-pentanol in the blend tended to minimize the knock resistance. Gautam et al. (25) showed that blending of higher alcohols in gasoline reduces specific emissions of CO, CO_2, and NO_x; however, they noted an increase in pentanal emissions as the *n*-pentanol blending concentration increased. Christensen et al. (27) recently reported that gasoline blending with *n*-pentanol reduces the octane rating of the fuel, and is therefore not an ideal fuel for displacing gasoline in spark ignition engines.

The aim of the present study is to provide a detailed kinetic model for *n*-pentanol which is suitable over a wide range of conditions. To our knowledge, the low-temperature chemistry of this fuel has not been previously investigated in detail. Providing insights into the detailed combustion chemistry of *n*-pentanol can help answer practical questions, such as why it has a lower octane rating than shorter alcohols and significant aldehyde (pentanal) emissions. For this purpose a recent C_4-alcohol model has been extended to simulate *n*-pentanol combustion, and this new model has been validated against various experimental data sets from the literature.

CHEMICAL KINETIC MODEL DEVELOPMENT. The proposed detailed chemical kinetic mechanism for *n*-pentanol builds upon a previous modeling study on the combustion of the butanol isomers (15, 28). A similar methodology and framework used in that study is applied here to develop a comprehensive model for *n*-pentanol, which includes both low-temperature and high-temperature kinetic pathways. Only a brief description of the model development process is discussed herein, and readers are referred to (15) and its supplementary material for a more detailed description of the methods employed. The thermodynamic data for *n*-pentanol and related radicals were calculated using the THERM program of Ritter and Bozzelli (29). The detailed chemical kinetic mechanism utilized in this work is based on the hierarchical nature of combustion mechanisms. Therefore, the reaction mechanism of *n*-pentanol was developed by adding its primary reactions and related radical reactions to the *n*-butanol reaction mechanism proposed by Sarathy et al. (15). The sub-mechanism for C_5 alkanes and alkenes taken from (30) is also included. The chemistry of C_5 aldehydes and enols was developed following the methods described in detail for C_4 aldehydes and enols in (15, 28). The entire model consists of 599 species and 3010 reactions. These input files are available as Supplemental Data to this publication. All the validation simulations were conducted using CHEMKIN PRO (31) with the appropriate reactor modules.

The reaction rates selected in this study follow directly from previous work on alkanes and alcohols. This approach was initially validated using quantum chemistry calculations to verify the most stable *n*-pentanol conformation and to obtain C–H and C–C bond dissociation energies. All geometry optimizations and frequency calculations were performed using the Gaussian09 suite of programs (32). The CBS-QB3 and G4 composite methods were selected for their reported accuracies of 1.0 and 1.1 kcal mol^{-1} (33, 34), respectively. Conformational analysis of *n*-pentanol, and bond-scission products were conducted to determine the most stable conformer of each species. Consistent with Moc et al. (35), the different conformers are labeled based on the dihedral angles along their backbone with a 'T' for a trans (180°) or a 'G' for gauche (60°) arrangement. Capital letters are used to refer to C–C–C–C or C–C–C–O dihedrals and lowercase letters are used for C–C–O–H (Figure S.1 in the Supplemental material). The CBS-QB3 and G4 methods differ in the absolute values for the BDE, with the G4 being consistently 2.2 ± 0.3 kcal mol^{-1} lower than the CBS-QB3 (refer to Table 1). However, because this deviation is consistent, the relative differences and general trends between the individual sites and conformations are nearly identical. The resulting CBS-QB3 values for the scission of a primary C–H bond (C_5–H in Table 1) and secondary C–H bond (C_4–H in Table 1) are closer to the values expected based on similar bonds in alkanes (36), while the values for OH, α, β, and γ sites (O–H, C_1–H, C_2–H, and C_3–H in Table 1) are consistent with CBS-QB3 calculated values for *n*-butanol (15, 28). The CBS-QB3 BDEs are therefore used to validate the corresponding values used in the model.

Consistent with Moc et al., who found the TGt conformer of butanol to be 0.3 kcal mol^{-1} lower in energy compared to the TTt conformer, the TTGt conformation of pentanol is 0.3 and 0.2 kcal mol^{-1} lower in energy than the TTTt conformer, according to the CBS-QB3 and G4 data sets, respectively (36). This trend continues for all of the radicals resulting from the bond-scission reactions (Table 1), where the C_3C_2–C_1O in a gauche conformation is 0.1–0.4 kcal mol^{-1} more stable than the same molecules in the trans configuration, at both 0 and 298 K, for both the CBS-QB3 and G4 methods.

The only exception to this is the O–H bond scission, in which the TTT conformation is 0.2 kcal mol^{-1} lower at 0 K but returns to the previous trend at 298 K with the TTG conformer being 0.1 kcal mol^{-1} lower. It should be noted that although the trend of the G configuration being lower in energy than the T for the C_3C_2–C_1O bond is the same for both of the high level composite methods, because the reported accuracy of each method is approximately 1.0 kcal mol^{-1} this difference cannot be confirmed and must wait for more accurate computational methods once they become viable.

The C–H and C–C BDEs exhibit significant dependence on their location relative to the oxygen site (Fig. 1). In particular, for both the C–C and C–H BDE values, those involving the production of a radical site on the α site that is still bound to the oxygen (the C_1–H and C_1–C_2 BDEs in Table 1) are consistently lower than the other values by roughly 4 kcal mol^{-1}, according to both of the G4 and CBS-QB3 methods. This weakening of the C–X bond is likely the result of the stability caused by the ability of an α-C radical to delocalize into the adjacent oxygen atom. Scission of the bonds that lead to the formation of a β-C radical (the C_2–H and C_2–C_3 bonds), on the other hand result in an increase in BDE. This increase is likely the result of steric interactions between the alcohol group and the sp2 hybridized radical site on C_2.

Table 1. Difference in enthalpy between two conformers of pentanol and the resulting bond dissociation energies of each conformer. Energies are relative to the TTGt conformation of pentanol (kcal mol^{-1}).

		CBS-QB3		G4	
Reaction	Conformer	ΔH (0 K)	ΔH (298 K)	ΔH (0 K)	ΔH (298 K)
Pentanol	TTGt	0.0	0.0	0.0	0.0
	TTTt	0.2	0.3	0.1	0.2
X-H bond scissions					
O–H bond scission	TTGt	103.9	104.7	101.8	102.6
	TTTt	103.7	104.8	101.8	102.7
C_1–H bond scission	TTGt	94.0	94.9	92.0	93.0
	TTTt	94.2	95.1	92.2	93.1
C_2–H bond scission	TTGt	98.8	100.0	97.0	98.1
	TTTt	98.9	100.1	96.9	98.1
C_3–H bond scission	TTGt	97.8	98.9	95.9	97.0

	TTTt	97.8	99.0	95.9	97.1
C_4–H bond scission	TTGt	97.4	98.6	95.4	96.6
	TTTt	97.6	98.9	95.6	96.9
C_5–H bond scission	TTGt	100.2	101.3	97.9	99.0
	TTTt	100.4	101.6	98.1	99.3
C-X bond scission					
C_1–O bond scission	TTT	93.9	95.0	91.2	92.3
C_1–C_2 bond scission	TT	85.9	86.8	83.6	84.5
C_2–C_3 bond scission	T, t	89.2	90.2	86.9	87.9
C_3–C_4 bond scission	Gt	87.7	88.7	85.5	86.5
	Tt	87.7	88.8	85.4	86.5
C_4–C_5 bond scission	TGt	88.1	89.5	85.5	86.9
	TTt	88.5	89.9	85.8	87.3

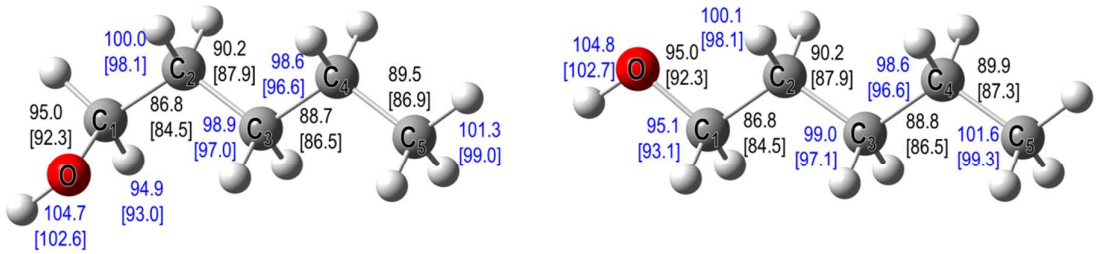

A) TTGt B) TTTt

Figure 1. Schematic diagram of the bond dissociation energies for Pentanol. A) TTgt configuration. B) TTTt configuration. The numbers in the brackets are G4 values, and those without the brackets are the CBS-QB3 values. Blue values are C–H and black are C–C BDEs (kcal mol^{-1} at 298 K).

Classes of reactions and rates. The major classes of elementary reactions considered for the oxidation of pentanol isomers are as follows:

High-temperature reaction classes

1. Unimolecular fuel decomposition
2. H-atom abstraction from the fuel

3. Fuel radical decomposition
4. Fuel radical isomerization
5. H-atom abstraction reactions from enols (i.e., unsaturated alcohols)
6. Enol-Keto tautomerizations and isomerizations catalyzed by H, HO_2, and formic acid
7. Addition of H atoms to enols
8. Enol radical decomposition
9. Unimolecular decomposition of enols
10. Reaction of O_2 with alpha-hydroxypentyl radicals to directly form an aldehyde + HO_2

Low-temperature reaction classes (R refers to a pentanol radical such as $CH_3CH_2CH.CH_2CH_2OH$ and QOOH refers to a hydroperoxy-pentyl-hydroxide radical such as $CH_3CH_2CH(OOH)CH_2CH.OH$)

11. Addition of O_2 to fuel radicals (R + O_2 = ROO)
12. R + ROO = RO + RO
13. R + HO_2 = RO + OH
14. R + CH_3O_2 = RO + CH_3O
15. ROO radical isomerization (ROO = QOOH) including Waddington type reaction mechanism
16. Concerted eliminations (ROO = enol + HO_2)
17. ROO + HO_2 = ROOH + OH
18. ROO + H_2O_2 = ROOH + HO_2

19. $ROO + CH_3O_2 = RO + CH_3O + O_2$

20. $ROO + ROO = RO + RO + O_2$

21. $ROOH = RO + OH$

22. RO decomposition

23. Formation epoxy alcohols via cyclization

24. $QOOH = enol + HO_2$ (radical site beta to OOH group)

25. QOOH = alkene/enol + carbonyl + OH (radical site gamma to OOH group)

26. Addition of O_2 to QOOH ($QOOH + O_2 = OOQOOH$)

27. Reaction of O_2 with alpha-hydroxypentylhydroperoxide radicals (e.g., $CH_3CH_2CH(OOH)CH_2CH.OH + O_2$)

28. Isomerization of OOQOOH and formation of carbonyl hydroxyalkyl-hydroperoxide species and OH including Waddington type reactions mechanism

29. Decomposition of carbonyl hydroxyalkyl-hydroperoxide species to form oxygenated radical species and OH

30. Cyclic oxygenates reactions with OH and HO_2

As mentioned previously, the CBS-QB3 values for the scission of primary and secondary C–H bonds are like values for similar bonds in alkanes, while the values for the OH, α, β, and γ sites are consistent with values for *n*-butanol. Similar trends exist for C–O and C–C bonds in the pentanol molecule. Therefore, Fig. 2 displays the alkane-like and alcohol-specific portions of the pentanol molecule, which forms the basis for the allocation of reaction rate constants. The channel-specific rates for high-temperature reaction classes 1–4 follow directly from analogies with *n*-pentane and *n*-

butanol. The subsequent low-temperature reaction pathways are also allocated rate constants based on our established rate rules for alkanes (37) and alcohols (15).

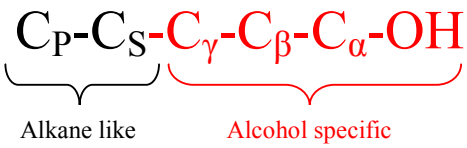

Figure 2. Treatment of the different carbon groups in n-pentanol.

The model developed in this way showed discrepancies when predicting low temperature auto ignition data for *n*-pentanol acquired in this study. To resolve these, the rate constant for reaction class 10 (i.e., O_2 with alpha-hydroxypentyl radicals to directly form an aldehyde + HO_2) was modified within its uncertainty bounds to better predict ignition delay times at the lowest temperatures. It should be noted that this reaction rate constant draws from previous work on *n*-butanol, which has only been tested against a limited set of ignition data. Additionally, the reaction rates for the R + O_2 system for butanol and pentanol systems have not been studied experimentally or theoretically, so the uncertainties in rate constants and branching ratios of various pathways are rather large. In this study, the high-pressure limit of the rate constant was decreased by a factor of 2.5, while the rate at all other pressures was increased by a factor of 2.5. Including reaction class 27 (O_2 with alpha-hydroxypentylhydroperoxide radicals) is critical for predicting the formation of pentanal-hydroperoxide species, as studied experimentally and theoretically by Perrin et al. (38). The rate constant for reaction class 27 was also modified to keep it in agreement with the rate constant for reaction class 10.

Transport Properties. The transport properties for new *n*-pentanol related species are determined as follows. For stable species, this study uses the correlations developed by Tee, Gotoh, and Stewart (39) as first described by Wang and Frenklach (40) for aromatics, and later by Holley and co-workers

for hydrocarbons (41, 42), to calculate the Lennard Jones collision diameter and potential well depth using the critical pressure (p_C), critical temperature (T_C), and acentric factor (ω). The estimation of the acentric factor (ω) is based on Lee-Kesler vapor-pressure relations, which requires the critical pressure (p_C), critical temperature (T_C), and boiling point (T_b) of the species.

Following previous work (43), the polarizability in cubic Angstroms of stable species is calculated using an empirical correlation (44), which depends on the number of C, H, and O atoms in the molecule. The dipole moment for *n*-pentanol is considered identical to *n*-butanol, which is a reasonable estimate because polarity is controlled by the hydroxyl functional group and not by the alkyl side chain. The index factor, which describes the geometry of the molecule, is determined from the molecular structure (i.e., 0 for atoms, 1 for linear molecules, and 2 for nonlinear molecules). All C_5 unsaturated oxygenates (e.g. enols, aldehydes, etc.) are assigned transport properties identical to pentanal (i.e., *n*-C_4H_9CHO). For hydroxypentyl radicals and pentenol radical species, the transport properties of their stable counterparts are used.

We also include a rough estimation of transport properties for species in the low temperature mechanism (i.e., RO, ROO, ROOH, QOOH, etc.) by assuming the transport properties are the same as the parent fuel molecule from which they are derived.

RESULTS AND DISCUSSION

Ignition delay times (IDT). Figure 3 presents the results from current kinetic simulations against experimental ignition delay time data (20) obtained in a high-pressure shock tube (ST) and in a rapid compression machine (RCM) at pressures between 9 and 30 bar at an equivalence ratio $\phi = 1.0$. Simulations have been performed using the CHEMKIN PRO (31) 0-D reactor software package. In order to include facility effects in the simulation, volume profiles have been deduced from pressure profiles measured in non-reacting experiments in the shock tube and in the rapid compression machine assuming an adiabatic compression/expansion process as suggested previously, e.g. (45).

The volume in the simulations is prescribed using these volume profiles which account for changes in pressure and temperature induced by facility effects. It can be seen in Fig. 5 that the pressure and temperature increase behind the reflected shock (p/p_5 = 7.25%/ms at 9 bar and p/p_5 = 5.5%/ms at 30 bar), due to shock attenuation, leads to shorter ignition delay times for long ignition delay times in shock tube experiments. In the rapid compression machine, heat loss effects induce a decrease in pressure and temperature after the end of compression leading to longer than expected ignition delay times when ignition delay times exceed about 20 ms, as discussed in more detail in (20). Overall the presented model, including facility effects, predicts well the experimental data. As expected, ignition delay times become shorter with increasing pressure. Within the intermediate-temperature regime, experimental data show an alkane-like NTC behavior, which is well reproduced by the kinetic model. For comparison to the current model, simulations with an *n*-pentanol kinetic model from the literature (21) are also presented in Fig. 3. This model was designed for lower pressures and lacks low-temperature chemistry, so that it fails to predict the ignition delay times observed in the present experiments.

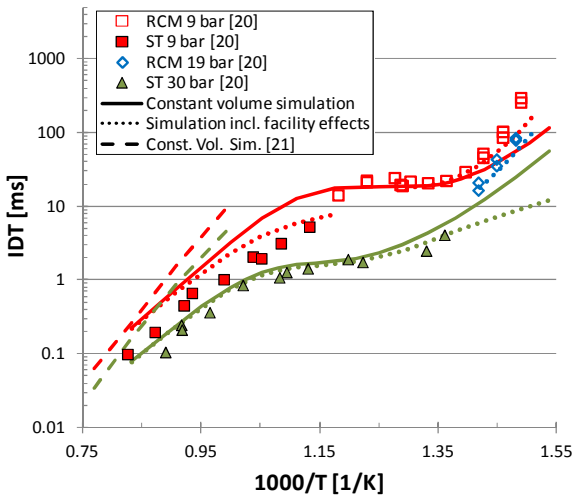

Figure 3. Comparison of experimental and predicted ignition delay times of n-pentanol-air mixtures at $\phi = 1.0$. Simulations at 9 bar are indicated by red curves, at 19 bar by blue curves, and at 30 bar by green curves.

It is interesting to note that *n*-butanol and *n*-pentanol show the same reactivity at high temperatures (Fig. 4). At these temperatures (> 1000 K), fuel decomposition and H-atom abstraction reactions at the alpha position by HO_2 are the most sensitive fuel-specific reactions influencing ignition delay times. Since the rates of these reactions can be assumed to be similar for both alcoholic fuels, this results in a similar reactivity at high temperatures, which is confirmed by the experimental results.

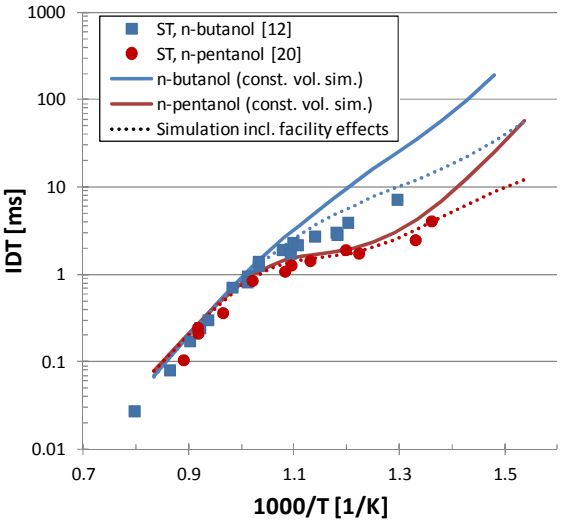

Figure 4. Comparison of ignition delay times at 30 bar and $\phi = 1.0$ for fuel/air mixtures of *n*-butanol and *n*-pentanol.

At low temperatures, *n*-butanol only shows a small indication of low-temperature reactivity (Fig. 4), while *n*-pentanol shows an alkane-like NTC behavior (Figs. 3, 4). It is interesting to note that the present modeling predictions of low-temperature autoignition behavior of *n*-pentanol are consistent with an engine-related study by Christensen et al. (27) who showed decreased octane ratings for gasoline blends containing *n*-pentanol. To understand the low-temperature behavior of these two alcohols, we investigated reaction pathways for *n*-butanol and *n*-pentanol (Fig. 5) at 30 bar and 700 K. We chose these conditions because high-pressures enhance low-temperature chemistry and at 700 K, the system is well into the low-temperature region. Current understanding of alkane chemistry suggests that the initial formation of hydroperoxalkyl (QOOH) radicals and subsequent

reaction with O_2 is required for low temperature chain branching (46, 47). Thus, it is important to know which reaction pathways and species lead to the formation of QOOH radicals. In general QOOH radicals are formed by internal isomerization from alkylperoxy (RO_2) radicals that are produced by the reaction of a fuel radical (R) with oxygen (O_2). The dominant source of fuel radicals is H-atom abstraction by OH radicals at these low temperatures. As can be seen in Fig. 5, the largest fraction of the fuel is converted into the alpha fuel radical. This is due to two effects. First, H-atom abstraction on the alpha-position is enhanced by the influence of the alcohol group compared to typical H-atom abstraction on *n*-alkanes. Second, the alcohol group inhibits H-atom abstraction on the beta- and gamma-positions resulting in slower reaction rates compared to secondary C-H sites in alkanes (20). In contrast to the typical alkane pathways, the reaction of the alpha fuel radical with oxygen mainly produces an aldehyde and HO_2 radical instead of RO_2 radicals, thus inhibiting chain branching. For this reason *n*-butanol and *n*-pentanol show a lower reactivity at low temperatures compared to their corresponding alkanes, i.e. *n*-butane and *n*-pentane. Reactions of the other fuel radicals with O_2 mainly lead to the formation of RO_2 radicals. The further internal isomerization to QOOH radical is in competition with the production of an enol, i.e., in this case butenol and pentenol, and HO_2 radical. In addition, the beta RO_2 radical can undergo a Waddington mechanism, which is also in competition with the formation of QOOH radicals. The Waddington pathway is a chain propagating route because it returns *one* OH radical to the initial radical pool, whereas internal isomerization leads to the formation of QOOH radicals which can eventually proceed to chain branching producing *two* OH radicals. In the case of *n*-butanol, the Waddington pathway competes with a 6-membered ring internal isomerization reaction involving a relatively stronger primary C–H site. However, for *n*-pentanol the Waddington mechanism competes with a 6-member ring internal isomerization from a relatively weaker secondary C–H site resulting in fewer RO_2 radicals proceeding through the Waddington mechanism. Therefore, initial H-atom abstraction from the beta site in *n*-pentanol eventually leads to more radical chain branching than the analogous pathway in *n*-butanol.

Nevertheless, this difference is of small importance for the overall reactivity since only a small amount of the fuel reacts through the beta-radical pathway. The major difference in reactivity between *n*-butanol and *n*-pentanol is due to the longer carbon chain length in the case of *n*-pentanol, which allows for H-atom abstraction on a secondary "alkane-like" carbon (delta position) to become possible. The formation of this fuel radical is significant faster than on the primary, beta, or gamma positions, such that it is competitive with H-atom abstraction on the alpha position. If the RO_2 undergoes internal isomerization to form QOOH through a six-membered ring, its addition to O_2 leads to significant chain branching (48). This explains the significant increase in reactivity for *n*-pentanol compared to *n*-butanol at low temperatures.

Another effect of the longer carbon chain in *n*-pentanol is that the 7-membered ring isomerization from an alpha-RO_2 radical to QOOH radical is faster than for *n*-butanol since it contains the easier H-atom abstraction on a secondary carbon site instead of on a primary one. This leads to a faster overall isomerization of the alpha-RO_2 radical to QOOH radical which enhances the pathway towards chain branching. At the same time, less pentanal and HO_2 radicals are formed by the reaction of the alpha-radical with molecular oxygen. Since this reaction is a major source of HO_2 radicals, H-atom abstraction by HO_2 radical on the alpha position is also significantly reduced leading to fewer alpha-fuel radicals.

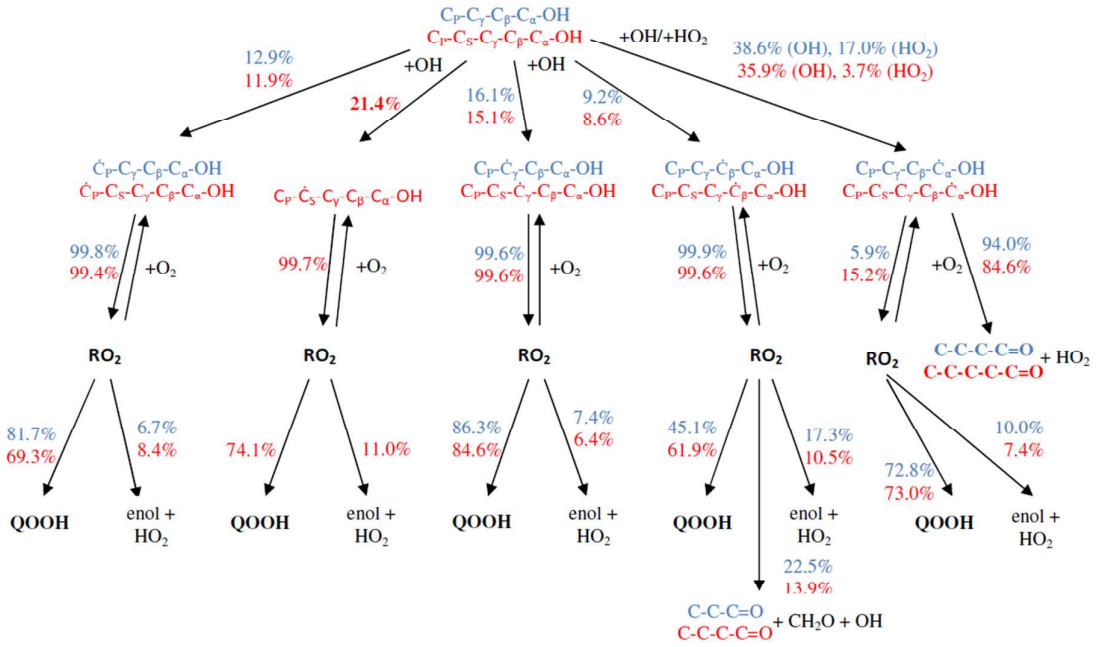

Figure 5. Reaction path analysis for *n*-butanol and n-pentanol at 700 K, 30 bar, $\phi = 1.0$. The reaction fluxes are given for 20% fuel consumption.

Table 2 shows the relative rate of production of QOOH radicals at 20% fuel consumption, where the percentage values of each radical are given relative to the total amount of fuel consumed. This again shows the difference between *n*-butanol and *n*-pentanol. For both fuels about 30% of the fuel reacts towards QOOH via the P, γ, β, and α channel. The additional S channel in *n*-pentanol leads to a significant higher production of QOOH radicals resulting in higher reactivity of *n*-pentanol at low temperatures.

Table 2: Production of QOOH via the different fuel radicals. The label indicates the position of the OOH group. When 6 and 7 membered-ring RO_2 isomerizations are possible, QOOH from both paths are lumped together.

	P	S	γ	β	α	∑
***n*-butanol**	10.5%	-	13.8%	4.1%	2.4%	30.8%
***n*-pentanol**	8.2%	15.8%	12.7%	5.3%	4.4%	46.4%

Jet-stirred reactor data. The following section presents a comparison between experimental data obtained in a jet-stirred reactor by Togbe et al. (21) and simulations performed with the proposed model. Experiments have been performed at 10 bar with a constant mean residence time of 0.7 s. As shown in previous studies (10, 36, 49, 50), a comparison between experiment and simulation at an equivalence ratio of ϕ = 1.0 is representative also for other equivalence ratios. For the simulation, the CHEMKIN PRO transient solver has been used to find the steady-state solution, with an end time of 20 s ensuring no change in the species mole fractions well before this time.

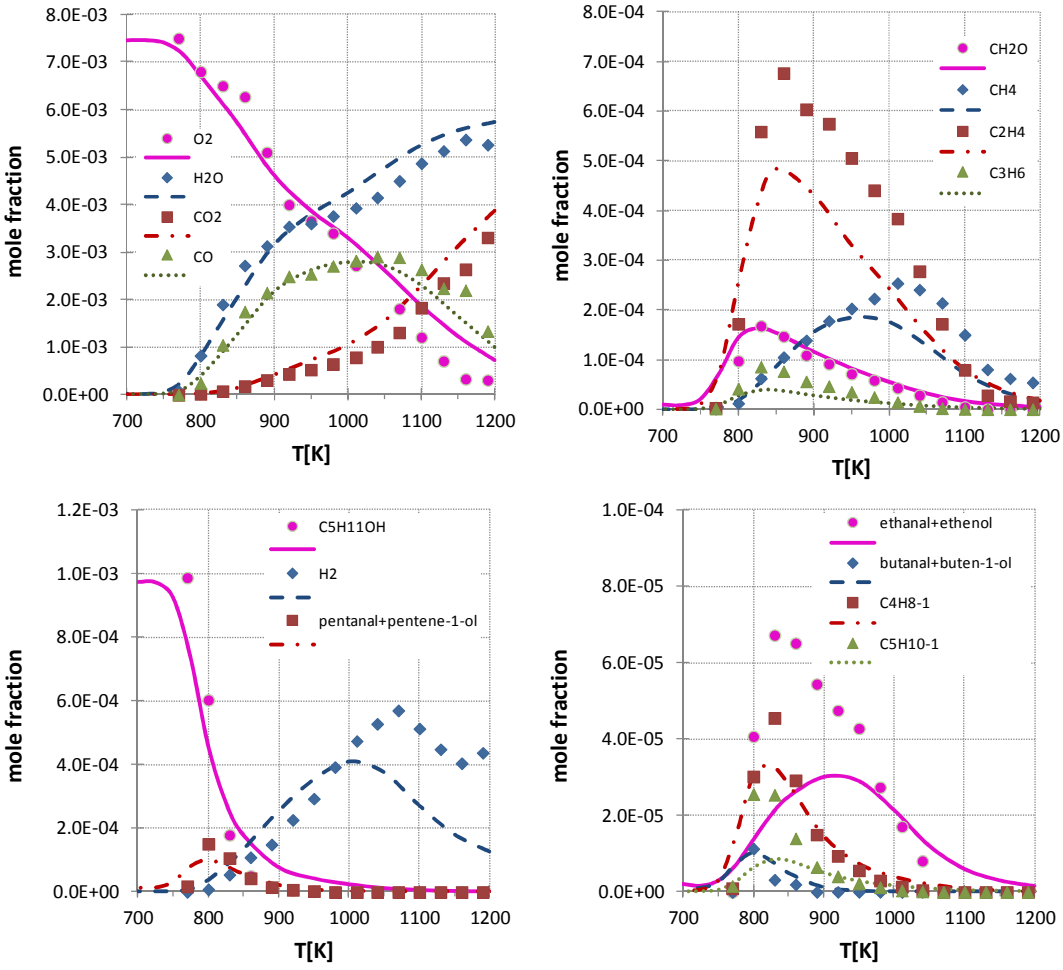

Figure 6. *n*-Pentanol oxidation in a JSR at 10 atm, s = 0.7 s and ϕ = 1. The initial fuel mole fraction was 0.1%. Experimental data (symbols) (21) are compared to simulations (lines).

Overall the agreement between simulation and experiment is very good (i.e., within a factor of 1.5–2.0) (Fig. 6). We present the model's summed prediction aldehydes plus enols because these species are indistinguishable in the experimental setup. The experimental profiles for the major species, i.e., oxygen, water, carbon monoxide and carbon dioxide, are especially well reproduced by the simulation. The maximum mole fraction of ethylene (C_2H_4) is under predicted by a factor of ~1.5 and that of propene (C_3H_6) by a factor of ~2.4. For hydrogen and methane, the maximum mole fractions are under predicted by a factor of ~1.5. The model under predicts 1-pentene (C_5H_{10}-1) concentration by more than a factor of two. This is an analogous trend that was observed previously in our butanol isomers modelling study (15), wherein 1-, 2-, and iso-butene concentrations were under predicted in the JSR. We attribute this under prediction to an uncertainty in the rate constant for the beta scission reaction $C_5H_{10}OH\text{-}2 <=> C_5H_{10} + OH$. The analogous reaction in *n*-butanol was also highlighted as an area requiring further experimental and/or theoretical research (16).

The model also does an excellent job at predicting oxygenated emissions. As noted earlier, the use of *n*-pentanol in engines leads to an increase in pentanal emissions (25). The model predicts that the major constituent of the C_5H_9O isomers produced in the JSR is pentanal, via the reaction of alpha-hydroxypentyl with molecular oxygen. Other important oxygenates include butanal, propanal, ethanal (i.e. acetaldehyde), and ethenol. The model predicts well the concentration of butanol and butenols, but under predicts the concentration of ethanal and ethenol by a factor of ~2.5 which we attribute to poorly understood ethenol oxidation chemistry. Consistent with our previous work on *n*-butanol (15), the *n*-pentanol model predicts that aldehydes are found in greater concentrations than their enol counterparts due to isomerization reactions catalyzed by H atom, HO_2 radical, and formic acid.

Premixed laminar flame velocity. In addition to the previously mentioned JSR data, measurements of laminar flame velocities of *n*-pentanol at atmospheric pressure have also been reported in (21). Simulations for predicting laminar flame velocities have been performed using the Premix flame

code in CHEMKIN PRO. For this purpose a high-temperature version of the model has been used wherein low-temperature chemistry reactions (Classes 11–30) have been removed. The simulations accounted for thermal diffusion (i.e., Soret effect), assumed mixture-averaged transport, and the solutions were highly resolved with approximately 200 grid points (GRAD 0.1, CURV 0.1). These simulations settings have been verified in a previous study (15).

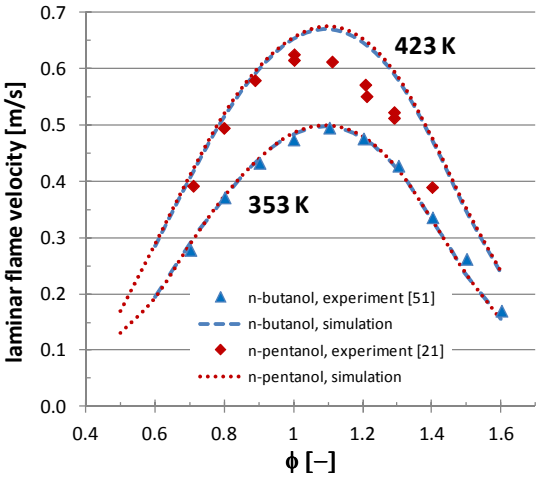

Figure 7. Predicted and experimental (21,51) atmospheric-pressure premixed laminar flame velocity for *n*-pentanol and *n*-butanol at different initial temperatures, experiments: symbols, simulations: lines.

Figure 7 shows experimental and simulation results for *n*-pentanol and *n*-butanol at atmospheric pressure. As shown in previous studies (15, 51), *n*-butanol exhibits the maximum laminar flame velocity at an equivalence ratio around $\phi = 1.1$ in experiments and simulations. From analogy with the behavior of alkanes (52), one would expect that the laminar flame speed is very similar for *n*-pentanol over the whole range of equivalence ratios. In fact the proposed model predicts more or less the same laminar flame velocity for *n*-pentanol as for *n*-butanol, under the same conditions. At higher initial temperatures the simulation predicts a faster laminar flame velocity than n-butanol, as expected, whereby the shape of the laminar flame velocity profile remains the same with the maximum flame velocity at around $\phi = 1.1$. Again, this behavior agrees well with the dependence on

initial temperatures and equivalence ratio observed for alkanes (52). However, the *n*-pentanol simulations only show good agreement with experimental data (21) at 423 K under lean conditions. The maximum laminar flame velocity is measured at an equivalence ratio of $\phi = 1.0$, and all fuel-rich data show slower laminar flame velocities than predicted by simulation. Refinements of the chemical kinetic model based on these experimental comparisons await confirmation from other experimental facilities.

CONCLUSIONS. This study presents a new kinetic model for *n*-pentanol. It is based on the application of reaction classes and rate constant rules, wherein the first three carbon sites adjacent to the alcohol group are treated like analogous sites in *n*-butanol, and the remaining carbon sites are treated like analogous sites in alkanes. Thus, the proposed model is a further extension of a previously published model of *n*-butanol. This new model has been validated against different experiments, i.e., ignition delay time measurements in shock tube and rapid compression machine, jet-stirred reactor species measurements, and laminar flame velocity measurements. Overall the model shows a good agreement to all experimental data. Compared to *n*-butanol, *n*-pentanol shows a significant increase in low temperature reactivity. This results from an alkane-like reaction pathway starting at a secondary carbon site, which is possible for *n*-pentanol but not for *n*-butanol. This reaction path leads to low temperature chain branching and is in direct competition with the largely inhibitory reaction sequence starting with H-atom abstraction from the alpha-carbon.

It has been shown that the applying reaction classes and rate rules for model development are valid and capable of describing the chemistry of alcoholic fuels with only minor adjustments needed to obtain good agreement with experimental data. Employing a similar method to that used in this study should make it possible to develop kinetic models for higher alcohols in future studies.

Nevertheless, certain reaction classes and rate constants rules, as highlighted in this study, warrant further experimental and/or theoretical investigation to reduce model uncertainties.

AUTHOR INFORMATION

Corresponding Author

* K. Alexander Heufer, Combustion Chemistry Centre, National University of Ireland Galway, University Road, Galway, Ireland, Alexander.heufer@nuigalway.ie, Tel.: +353 91 492579

ACKNOWLEDGEMENT

The work performed at the Clean Combustion Research Center acknowledges research funding from the King Abdullah University of Science and Technology. The work performed at LLNL was performed under the auspices of the US Department of Energy under Contract DE-AC52-07NA27344.

ASSOCIATED CONTENT

Supporting Information. The kinetic mechanism, associated thermochemistry, and transport data used here in CHEMKIN format, schematic diagram of the select geometric parameters for pentanol, and Cartesian coordinates for the CBS-QB3 geometry optimizations. This material is available free of charge via the Internet at http://pubs.acs.org.

REFERENCES

(1) Kohse-Hönighaus, K.; Osswald, P.; Cool, T. A.; Kasper, T.; Hansen, N.; Qi, F.; Westbrook, C. K.; Westmoreland, P.R.; *Angew. Chem. Int. Ed.* **2010,** *49,* 3572–3597.
(2) Dunphy, M. P.; Simmie, J. M.; *Journal of the Chemical Society, Faraday Transactions* **1991,** *87*, 1691–1696.
(3) Curran, H. J.; Dunphy, M.; Simmie, J. M.; Westbrook, C. K.; Pitz, W. J.; *Proc. Comb. Inst.* **1992**, *24,* 769–776.
(4) Marinov, N. M.; *Int. J. Chem. Kinet.* **1999**, *31*, 183–220.

(5) Li, J.; Kazakov, A.; Chaos, M.; Dryer, F. L.; 5th US Combustion Meeting, paper C26, San Diego, USA, 2007
(6) Heufer, K. A.; Olivier, H.; *Shock Waves* **2010**, *20*, 307–316.
(7) Leplat, N.; Dagaut, P.; Togbé, C.; Vandooren, J.; *Combust. Flame* **2011**, *158*, 705–725.
(8) Lee, C.; Vranckx, S.; Heufer, K. A.; Khomik, S.; Uygun, Y.; Olivier, H.; Fernandes, R.X.; *Zeitschrift für Physikalische Chemie* **2012,** *226*, 1.
(9) Miller, G. L.; Smith, J. L.; Workman, J. P.; *Trans. ASAE* **1981**, *24*, 538–540.
(10) Sarathy, S. M.; Thomson, M. J.; Togbé, C.; Dagaut, P.; Halter, F.; Mounaim-Rousselle, C.; *Combust. Flame* **2009**, *156*, 852–864.
(11) Hansen, N.; Harper, M. R.; Green, W. H.; *Phys. Chem. Chem. Phys.* **2011**
(12) Heufer, K. A.; Fernandes, R. X.; Olivier, H.; Beeckmann, J.; Roehls, O.; Peters, N.; *Proc. Combust. Inst.* **2010**, *33*, 359–366.
(13) Black, G.; Curran, H. J.; Pichon, S.; Simmie, J. M.; Zhukov, V.; *Combust. Flame* **2010**, *157*, 363–373.
(14) Heufer, K. A.; Olivier, H.; Vranckx, S.; Lee, C.; Fernandes, R. X.; Experimental study of the high-pressure ignition of alcohol based biofuels. European Combustion Meeting 2011at Cardiff, United Kingdom, 2011.
(15) Sarathy, S. M.; Vranckx, S.; Yasunaga, K.; Mehl, M.; Oßwald, P.; Metcalfe, W. K.; Westbrook, C. K.; Pitz, W. J.; Kohse-Hönighaus, K.; Fernandes, R. X.; Curran, H.J.; *Combust. Flame* **2012**, *159*, 2028–2055.
(16) Cann, A. F.; Liao, J. C.; *Apll. Microbiol. Biotechnol.* **2010**, *85*, 893–899.
(17) Zhang, K.; Sawaya, M. R.; Eisenberg, D. S.; Liao, J.C.; *Proc. Natl. Acad. Sci. USA* **2008**, *105,* 20653–20658.
(18) Lachenmeier, D. W.; Haupt, S.; Schulz, K.; *Regul. Toxicol. Pharmacol.* **2008**, *50*, 313–321.
(19) Oliveira, J. M.; Faria, M.; Sa, F.; Barros, F.; I.M. *Araujo, Anal. Chim. Acta* **2006**, *563*, 300–309.
(20) Heufer, K.A.; Bugler, J.; Curran, H.J.; *Proc. Combust. Inst.* **2012**, in press, http://dx.doi.org/10.1016/j.proci.2012.05.103
(21) Togbe, C.; Halter, F.; Foucher, F.; Mounaim-Rousselle, C.; Dagaut, P.; *Proc. Comb. Inst.* **2011**, *33,* 367–374.
(22) Togbe, C.; Dagaut, P.; Mze-Ahmed, A.; Dievart, P.; *Energy Fuels* **2010**, *24*, 5859–5875
(23) Aloko, D.; Adebayo, G. A.; Oke, O. E., *Leonardo Electronic Journal of Practices and Technologies* **2007**, 151–156.
(24) Raj, C. S.; Edward, I. R.; Nimosh, J.; Mon, G. N.; Rameez, Y. M., *Int. J. Appl. Eng. Res.* **2010**, *5*, 7.
(25) Gautam, M.; Martin, D.W.; *Proc. Instn. Mech. Engrs. Part A* **2000**, *214*, 165–182.
(26) Gautam, M.; Martin, D.W.; Carder, D.; *Proc. Instn. Mech. Engrs. Part A* **2000**, *214*, 497–511.
(27) Christensen, E.; Yanowitz, J.; Ratcliff, M.; McCormick, R.L.; *Energy Fuels* **2010**, *25*, 4723–4733.
(28) Yasunaga, K., Mikajiri, T.; Sarathy, S.M.; Koike, T.; Gillespie, F.; Nagy, T.; Simmie, J. M.; Curran, H. J.; *Combust. Flame* **2012**, *159*, 2009-2027.
(29) Ritter, E.; Bozelli, J.; *Int. J. Chem. Kinet.* **1991**, *23*, 767.
(30) Healy, D.; Kalitan, D. M.; Aul, C. J.; Petersen, E. L.; Bourque, G.; Curran, H.J; *Energy Fuels* **2010**, 24, 1521–1528
(31) CHEMKIN-PRO Release 15101, Reaction Design, Inc., San Diego, CA, 2010.
(32) Frisch, M.J.; Trucks, G. W.; Schlegel, H. B.; Scuseria, G. E.; Robb, M. A.; Cheeseman, J. R.; Scalmani, G.; Barone, V.; Mennucci, B.; Petersson, G. A.; Nakatsuji, H.; Caricato, M.; Li, X.; Hratchian, H. P.; Izmaylov, A. F.; Bloino, J.; Zheng, G.; Sonnenberg, J. L.; Hada, M.; Ehara, M.; Toyota, K.; Fukuda, R.; Hasegawa, J.; Ishida, M.; Nakajima, T.; Honda, Y.; Kitao, O.; Nakai, H.; Vreven, T.; Montgomery, Jr., J. A.; Peralta, J. E.; Ogliaro, F.; Bearpark, M.; Heyd, J. J.; Brothers, E.; Kudin, K. N.; Staroverov, V. N.; Kobayashi, R.; Normand, J.; Raghavachari, K.; Rendell, A.; Burant, J. C.; Iyengar, S. S.; Tomasi, J.; Cossi, M.; Rega, N.; Millam, N. J.; Klene, M.; Knox, J. E.; Cross, J. B.; Bakken, V.; Adamo, C.; Jaramillo, J.; Gomperts, R.; Stratmann, R. E.; Yazyev, O.; Austin, A. J.; Cammi, R.; Pomelli, C.; Ochterski, J. W.; Martin, R. L.; Morokuma, K.; Zakrzewski, V. G.; Voth, G.

A.; Salvador, P.; Dannenberg, J. J.; Dapprich, S.; Daniels, A. D.; Farkas, Ö.; Foresman, J. B.; Ortiz, J. V.; Cioslowski, J.; Fox, D. J.; *Gaussian 09* **2009**, Gaussian, Inc.: Wallingford CT
(33) Montgomery, J. A.; Frisch, M.J.; Ochterski J. et al., *J. Chem. Phys.* **2000**, *112*, 6532-6542.
(34) Curtiss, L.A.; Redfern, P. C.; Raghavachari, K.; *J. Chem. Phys.* **2007**, *126*, 084-108.
(35) Moc, J.; Simmie, J.M.; Curran, H.J.; *J.Molec.Struct.* **2009**, *928*, 149–157.
(36) Castelhano, A.L; Griller, D.; *J. Am. Chem. Soc.* **1982**, *104*, 3655.
(37) Sarathy, S.M.; Westbrook, C.K.; Mehl, M.; Pitz, W.J.; Togbe, C.; Dagaut, P.; Wang, H.; Oehlschlaeger, M. A.; Niemann, U.; Seshadri, K.; Veloo, P.S.; Ji, C.; Egolfopoulos, F.N.; Lu, T.; *Combust. Flame* **2011**,*158,* 2338–2357
(38) Perrin, O.; Heiss, A.; Doumenc, F.; Sahetchian, K.; *J. Chem. Soc., Faraday T rans.* **1998**, *96,* 2323-2335.
(39) Tee, L.S.; Gotoh, S.; Stewart, S.; *Ind. Eng. Chem. Fundam.* **1966**, *5*, 356–363.
(40) Wang, H.; Frenklach, M.; *Combust. Flame* **1994**, *96*, 163–170.
(41) Holley, A.; You, X.; Dames, E.; Wang, H.; Egolfopoulos, F.; *Proc. Combust. Inst.* **2009**, *32*, 1157–1163.
(42) Holley, A.; Dong, Y.; Andac, M.; Egolfopoulos, F.; *Combust. Flame* **2006**, *144*, 448–460.
(43) Sarathy, S. M.; Thomson, M. J.; Pitz, W. J.; Lu, T.; *Proc. Combust. Inst.* **2011**, *33,* 399–405.
(44) Bosque, R.; Sales, J.; *J. Chem. Inf. Model.* **2002**, *42*, 1154–1163.
(45) Chaos, M.; Dryer, F.L.; *Int. J. Chem. Kin.* **2010**, *42*, 143–150.
(46) Curran, H. J.; Gaffuri, P.; Pitz, W. J.; Westbrook, C. K.; *Combust. Flame* **1998**, *114*, 149-177.
(47) Wang, S.; Miller, D. L.; Cernansky, N. P.; Curran, H. J.; Pitz, W. J.; Westbrook, C. K.; *Combust. Flame* **1999**, *118*, 415-430.
(48) Pitz, W. J.; Naik, C. V.; Mhaolduin, T. N.; Westbrook, C. K.; Curran, H. J.; Orme, J. P.; Simmie, J. M.; *Proc. Combust. Inst.* **2007**, *31*, 267-275.
(49) Dayma, G.; Gaïl, S.; Dagaut, P.; *Energy Fuel* **2008**, *22*, 1469–1479.
(50) Gaïl, S.; Thomson, M.; Sarathy, S.; Syed, S.; Dagaut, P.; Diévart, P.; Marchese, A.; Dryer, F.; *Proc. Combust. Inst.* **2007**, *31*, 305–311.
(51) Liu, W.; Kelley, A.; Law, C.; *Proc. Combust. Inst.* **2011**, *33*, 995–1002.
(52) Ji, C.; Dames, E.; Wang, Y. L.; Wang, H.; Egolfopoulos, F.N.; *Combust. Flame* **2010**, *157*, 277–287.